ICE Research and Development Enabling Fund - FEMDEM Project Report

ice

**Institution of Civil Engineers**

Research and Development Enabling Fund

Final Report

# Simulation of fracture propagation in fibre-reinforced sprayed concrete lined tunnels using FEMDEM

A. Farsi, A. Bedi, J.P. Latham and K. Bowers

January 2018

**Final Report**

**ICE Research and Development**
**Enabling Fund - FEMDEM**
**Project Report**
**January 2018**

# Simulation of fracture propagation in fibre-reinforced sprayed concrete lined tunnels using FEMDEM

A. Farsi

Applied Modelling and Computation Group,
Department of Earth Science and Engineering
Imperial College London, SW7 2AZ, United Kingdom

A. Bedi

Bedi Consulting Ltd

J.P. Latham

Applied Modelling and Computation Group,
Department of Earth Science and Engineering
Imperial College London, SW7 2AZ, United Kingdom

K. Bowers

London Underground Limited

**Abstract:** In this research, the application of the combined finite-discrete element method (FEMDEM) to simulate fracture propagation in fibre-reinforced-sprayed-concrete (FRSC) lined tunnels has been investigated. This work constitutes the first attempt of using FEMDEM for the simulation of fracture in FRSC structures. For this reason, a new joint-element constitutive model for fibre-reinforced concrete has been implemented and validated with three-point bending experimental data. The code has also been applied to a practical tunnel design case study. The final aim is to better understand the post-crack behaviour of FRSC linings. The ultimate objective of this research is to better understand the fracture mechanics and crack propagation behaviour of FRSC tunnels. The novel techniques employed in this study will help to increase knowledge of the serviceability and ultimate limit state behaviour of FRSC tunnel linings, and so significantly contribute to the development of detailed design guidance for FRSC structures. Although the case studies proposed in this work have been limited to FRSC tunnels, the results of this research can be applied to any FRC structure.

# Table of Contents

# List of Figures

# Acknowledgements

This research is the result of a collaboration between Dr A. Farsi (Imperial College London), Dr J.P. Latham (Imperial College London) Dr K. Bowers (London Underground) and Dr A. Bedi (Bedi Consulting). This work has been sponsored by the Institute of Civil Engineers (ICE).

# 1 Introduction

Following the collapse of the Heathrow Express Rail Link tunnel in 1994 (and 39 other major SCL tunnel collapses world-wide), a review by the Health & Safety Executive [4] concluded that some safety-critical aspects of SCL design and construction were poorly understood. Two notable deficiencies identified by the HSE were: a) the approximate nature of the method of analysis (semi-empirical methods) used in SCL design, and; b) the considerable uncertainty in the behaviour of the materials that constitute the SCL. These introduce numerous uncertainties in a typical tunnel project that can interact in a complex manner. The HSE report conclude that: "*At present, it is impractical to prepare calculations for the construction of a tunnel which takes sufficient account of the complexity of the properties of the ground, the ground support system (the SCL) and the geometry of intermediate phases of construction. Therefore, despite their apparent rigour, the design calculations will be approximate and may not accurately represent conditions in the ground and tunnel. The uncertainty is due to the limits of current technology and can only be overcome by further research.*" (pp.80).

Adding to the complexities identified by the HSE, an industry objective to increase safety by removing operatives working beneath unsupported ground has seen the conventionally bar reinforced SCL replaced with fibre-reinforced-sprayed-concrete (FRSC). Compared to conventional steel bar or mesh reinforced linings that are designed using well-accepted methods for reinforced concrete structures, normative design codes for FRSC design are still being developed for this relatively new material.

The fracture behaviour of FRSC tunnel linings is thus currently not well understood, and this has led to significantly increased SCL thicknesses and sub-optimal designs. Current state-of-the-art industry practice involves modelling SCL tunnels using elastic elements in a continuum approach (i.e. Finite Element Modelling). However, this method does not effectively capture the post-crack behaviour of FRSC linings. While this approach has been successful in improving the safety of SCL tunnel construction, it is widely accepted that the resulting designs may be overly conservative.

This research aims to provide an insight into design approaches that could be applied in the future to optimise the tunnel linings, whilst ensuring the safety of these structures. Consequently, this work may lead to substantial cost saving on the numerous, large-scale SCL tunnelling projects proposed in London and in the UK.

## 1.1 Objectives

The ultimate objective of this research is to better understand the fracture mechanics and crack propagation behaviour of FRSC tunnels. With the mandatory introduction of limit state design in the Eurocodes for the design of geotechnical structures, it is envisaged that the novel techniques employed in this study will increase knowledge of the serviceability and ultimate limit state behaviour of FRSC tunnel linings, and so significantly contribute to the development of detailed design guidance for FRSC structures.

In order to achieve these objectives, the combined finite-discrete element method (FEMDEM) analysis will initially aim to simulate the fracture behaviour of plain concrete and FRSC. The next goal of the research will be to understand the complex interaction between the lining and the ground, in which the ground both loads and supports the lining.

The lining relies upon the ground to prevent damaging deformation; if this displacement exceeds the strain capacity of the lining, the structure will crack. To prevent a collapse, the lining must be able to support the hoop load as rotation occurs at the crack.

Because FEMDEM methodology models deformation of continua, the transition from the continua to discontinua through crack initiation, and multibody interaction of the discrete fragments, post-crack displacements and collapse modes can be accurately simulated. The proposed FEMDEM analysis aims to capture these mechanisms and so improve the results obtained from the potentially conservative current continuum methods, which do not explicitly capture crack initiation and propagation and consequent stress redistribution.

## 1.2 Methodology

In this research, a new joint-element constitutive model for fibre-reinforced concrete has been defined. The new joint-element constitutive model has been calibrated against published experimental data in order to validate the code.

The current FEMDEM constitutive model for elastic brittle materials has been implemented based on a Mohr-Coulomb failure criterion with tension cut off (Figure 1(a)) with the stress-strain behaviour consisting of a linear elastic

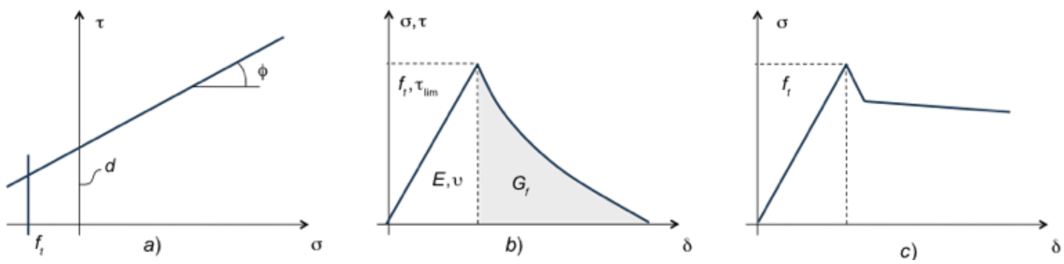


Figure 1. FEMDEM implementation of joint-element constitutive model.

branch up to the peak stress, followed by a strain-softening response where stress decreases with the strain increasing (Figure 1(b)).

The post peak behaviour is defined in the code in terms of stress and displacements of the joint-elements (i.e. cohesive elements that are located in between each couple of edges of the finite element mesh) to allow the transition from continua (before failure) to discontinua (fragmentation).

In the proposed study, the elastic-brittle joint element constitutive model has been modified to obtain a linear elastic response until failure followed by a bi-linear softening curve, which is more akin to the post peak softening behaviour usually seen in fibre reinforced concrete (Figure 1(c)).

Validation of the implemented constitutive model has been undertaken through simple benchmark problems. This step validates that the joint element constitutive model is representative of the expected behaviour, and can be confidently applied to a practical application. The software has then been applied to practical tunnel design case studies. The FEMDEM code has been able to capture the failure mechanisms of the analysed FRSC tunnel linings.

# 2 Design of fibre reinforced concrete

Although FRSC has been used in the UK and elsewhere for a number of years, there are no agreed design approaches for many of the current applications. This differs from conventional reinforced concrete using steel bars or welded fabric, which has been covered by national and international design codes for many years.

The reason for this is due to the inherent variability in the macro-mechanical properties which constitutes the FRSC member. As fibres are manufactured in a variety of shapes and materials (e.g. Figure 2(a)), some the physical characteristics of fibres such as: bond and anchorage mechanisms (e.g. straight or deformed shape, end cones or hooked ends); fibre length and diameter, and hence the aspect ratio; dosage (kg/m$^3$); tensile strength, and; Elastic modulus directly affect key aspects of concrete performance while others are less important.

In addition to this, the behaviour of a concrete element that incorporates fibres is more critical than the properties of the fibres themselves. It is the combined response of the concrete and fibre interaction that affects the stress-deflection-cracking behaviour of the FRSC element (see Figure 2(b)).

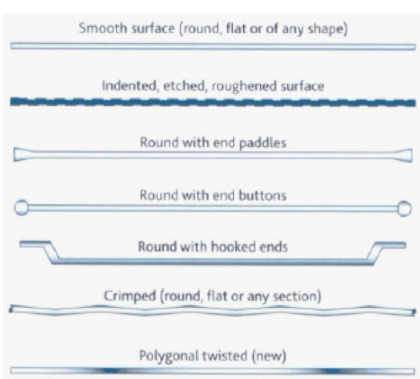


(a)

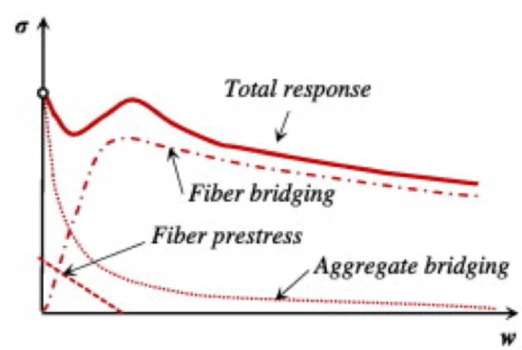


(b)

Figure 2. a) Types of steel fibres. b) Constitutive models ($\sigma$-w) for the tensile response of FRC [6].

For this reason, design standards, e.g. BS EN 14889-1[5], have been introduced to quantify the effect of fibres on the strength of concrete in accordance with standardised test methods e.g. the standard notched beam test in BS EN 14651[1] (See Figure 2(a)).The testing is required to determine the amount of fibres in kg/m$^3$ required to achieve the specified residual (post-cracking) flexural strength at varying levels of crack mouth opening displacement (CMOD). The output from such tests is a characteristic stress-deflection-crack curve for a specific SFRC mix (Figure 2(b)). Once the load-CMOD characteristics of the SFRC mix have been determined through testing, various design approaches can be adopted to calculate the load carrying capacity of the FRSC member.

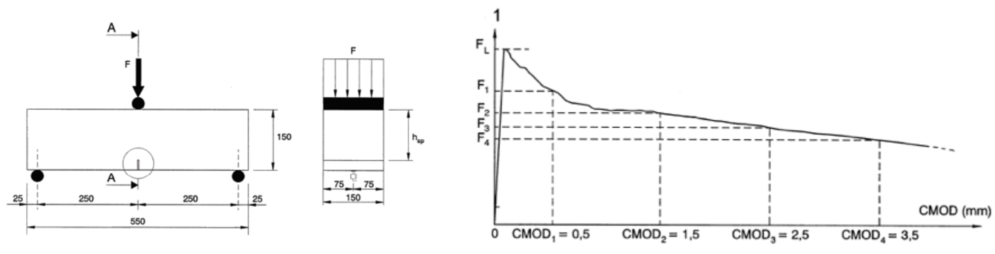


(a) (b)

Figure 3. a) Three-point bending test. b) Typical Load-CMOD diagram from bending test [1].

## 2.1 FRSC stress-strain model

Concrete is a brittle material with a low tensile strength. Adding steel fibres to concrete enhances its toughness, ductility and energy absorption capacity under impact. However, at normal dosages, fibres do not affect the flexural strength of the concrete but provide a degree of post-cracking load-carrying capacity through the following mechanisms:

1. Fibres, being randomly distributed in the concrete, intercept micro-cracks as they form, inhibiting the tendency for them to form into larger cracks.

2. After cracking, the fibres spanning the crack will provide a degree of residual load carrying capacity. This capacity can be considerable, depending on the dosage and the type of fibre used, and can be used in plastic design approaches.

The idealised stress-strain response of FRSC in compression and tension is shown in Figure 4(a). The compressive behaviour of concrete is usually defined by a non-linear elastic, brittle post-peak. In tension, the concrete is assumed linear elastic until first crack, followed by a bi-linear strain softening response.

The load deflection response in tension is reproduced in Figure 4(b), and is known as strain softening since the flexural resistance reduces with increasing deformation after cracking. This type of behaviour differs from that of reinforced concrete where the flexural resistance increases after cracking, provided that the minimum amount of reinforcement specified in structural design codes is provided. The strain softening response invalidates many of the simplifying assumptions conventionally made in the design of reinforced concrete.

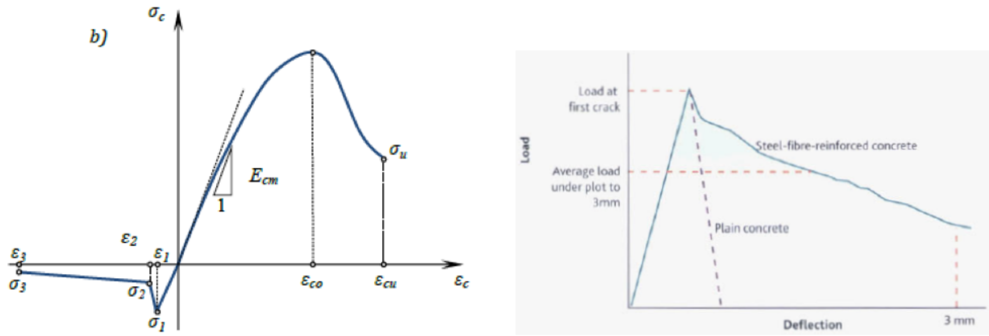


(a) (b)

Figure 4. a) Typical stress-strain response of FRSC. b) Load-Deflection response of FRSC in tension.

## 2.2 Design methods

While there is no normative design standard for FRSC in the U.K. or the EU, the increased incorporation of fibres as a reinforcing material has seen the publication of design guidance and recommendations in Europe, namely: the German "DBV" code [7], the RILEM Scientific Committee 162 recommendations [8], the Italian guideline [9], the Spanish code [10] and most recently the *fib* Model Code [11].

### 2.2.1 Ultimate Limit State (ULS)

Within these codes and guides, the material properties such as residual tensile strength determined from standard small beam or statically determinate slab tests are inserted into equations defining the performance of the concrete element to determine the load capacity.

This is similar to the approach adopted by reinforced concrete design codes such as and Eurocode 2 [12]. In general, the design equations are linked to properties determined from a specific test. One advantage of this approach is that the equations are general and are not specific to any particular material.

Whilst the different approaches proposed to address the tensile behaviour of FRC are capable of providing conservative estimates of ultimate load carrying capacity, at present it appears they may not be sufficiently developed to predict stress re-distribution and over-load behaviour at large strains and crack widths.

### 2.2.2 Serviceability Limit State (SLS)

Although there is no suitable design approach for estimating crack widths in structures reinforced with fibres only, experience has shown that fibres can be beneficial in limit the widths of cracks. At present crack widths can be estimated using the simplified methods given in the either the RlLEM recommendations or *fib* Model code.

However, it is impossible to reliably predict crack widths in SFRC structures without conventional reinforcement since the crack widths are not related to stresses given by elastic analysis once the section capacity is exceeded and softening develops. In some circumstances, it may be necessary to control crack widths to prescribed limits, and given the uncertainty in the crack prediction models, consideration is usually given to providing conventional reinforcement in addition to steel fibres to control crack widths.

It is for all the above reasons that there is considerable interest in exploring numerical approaches to simulate fracture propagation in FRSC structures.

# 3 Simulating fracture propagation

Interest in simulating fracture propagation extends across a variety of scientific and engineering fields, such as structural analysis, material design, nuclear waste disposal risk assessment, oil and gas reservoir engineering, and subsurface ore mining [13]. Numerical simulations are performed in order to predict the formation and behaviour of these fracture systems, due to the geometric and physical complexity inherent in fracture phenomena.

Two main modelling approaches can be identified in the literature for fracture analysis: discrete crack and smeared crack models, also known as geometric/non-geometric, or grid/subgrid methods. They were introduced in the late 1960s by Ngo and Scordelis and Rashid in application to the concrete structural analysis [14]. The smeared crack model is based on the assumption that in concrete, due to its heterogeneity and the presence of reinforcement, many small cracks nucleate which only in a later stage of the loading process link up to form one or more dominant cracks. Since each individual crack is not numerically resolved, the smeared crack model captures the deterioration process through a constitutive relation, thus smearing out the cracks over the continuum. In this kind of analysis cracks are represented as an isotropic or anisotropic damage concentration band within a mesh element from which fracture geometry can be inferred, instead of being explicitly defined [15]. In contrast, the discrete crack model represents cracks discretely and aim to simulate the initiation and propagation of dominant cracks. This kind of analysis can be performed with different approaches, e.g. boundary element based methods (BEM) [16], peridynamics [17, 18], finite element simulations (FEM) [19, 20] extended finite element method (XFEM) [21], discrete element method (DEM) [22, 23, 24, 25, 26] or combined finite-discrete element method (FEMDEM) [2]. An important aspect to underline is that the great majority of geometric methods do not maintain a representation of the fractures separate from the mesh, and rely on mesh editing techniques, such as in situ insertion of new crack nodes, edges and faces, to capture mesh growth.

There are also several approaches presented in the literature aimed at describing solid fragmentation using DEM. In [24] numerical simulations of uniaxial compression and cutting processes of rock have been presented employing packed discrete elements bonded together to represent the bulk rock material. Similar examples are presented to describe tunnelling, flexural and Brazilian tests in [26]. The standard approach consists of defining a packed structure of particles (generally spheres) with a determined particle size distribution and then defining laws for the contact and interactions between particles on the basis of parameters such as penalty numbers, stiffness of the bonding, etc. and to obtain forces that, once they are applied to the elements, define the movement of the simulated bodies with Newton's laws of motion.

Algorithms for FEMDEM simulations started to be proposed from the 90s. Extensive developments and applications of the FEMDEM method have been carried out after the release of the open source Y-code in [2], and different versions have been released, including the code developed from the collaboration between Queen Mary University and Los Alamos National Laboratory [27, 28], the Y-Geo and Y-GUI software that have been developed by the Geomechanics Group led by Giovanni Grasselli at Toronto University [29, 30], and VGeST (Virtual Geoscience Simulation Tools) released by the Applied Modelling and Computation Group (AMCG) at Imperial College London [31, 32]. Recently the AMCG has upgraded and renamed VGeST as 'Solidity'. A commercial FEMDEM code developed by Geomechanica (www.geomechanica.com), has also been released in Canada, although its application has been limited to modelling geomaterials. While the first Y-code employed finite strain elasticity coupled with a smeared crack model to capture deformation, rotation, contact interaction and fragmentation, the AMCG has greatly improved the code, implementing a range of constitutive models in 3D [33, 34], thermal coupling [35], parallelisation and a faster contact detection algorithm [36].

Several models for the simulation of fibre-reinforced concrete have been proposed [37, 38, 39]. Most of the techniques that have been presented, instead of inserting discrete fractures, represent the concrete failure in a continuous fashion with plastic deformations. In [3] a cohesive fracture model for the simulation of FRC has been presented. One of the limitations of this approach is that the locations of the fractures must be known a priori in order to insert cohesive elements in the right locations in the model. One of the main advantages of using FEMDEM is that fractures can initiate anywhere in the simulated system, without the need of knowing the failure mechanism a priori.

# 4 Fracture initiation and propagation in FEMDEM

## 4.1 Plain concrete

The Y-code, which was presented in [2], has provided the fundamental theoretical aspects of the contact and cohesive crack model employed in this work. The transition from a continuous domain to a discontinuous domain is carried out through fracture initiation and propagation processes. The progressive fracture mechanisms implemented in the code for the description of plain concrete is idealised with a distributed micro-crack zone, a bridging zone, and a traction free macro-crack zone. This is based on the assumption that the stress-strain curved consists of a hardening branch (before the peak) and a strain-softening part (where the stress decreases with the strain increasing), as illustrated in Figure 5.

Figure 6 shows the strain-softening relation that has been implemented in the code through the constitutive law of the joint elements in terms of stress and displacements. The strain-softening part is also defined in terms of stress and displacements in order to avoid the ill-posedness of the problem generated by a stress-strain definition. The area under the graph in Figure 6 is the energy release rate ($G_c$), i.e. the energy dissipated in order to extend the surface of the crack. $G_c$ is also equal to twice the surface energy, which quantifies the disruption of bonds that occur when a surface is created. The relationship between stresses and displacements is modelled through a single crack model: when the size of separation is zero the bonding stress is equal to the tensile strength ($f_t$), implying that the separation begins only after reaching this

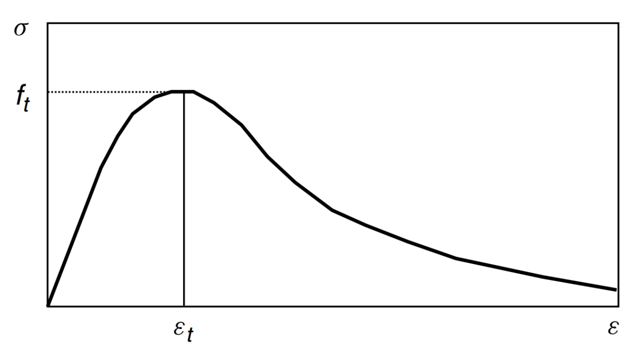


Figure 5. Objective stress-strain curve to be modelled for the plain concrete [2].

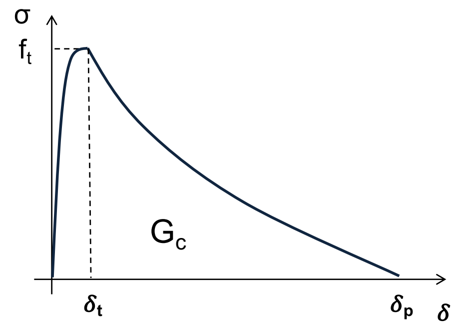


Figure 6. Strain softening defined in terms of displacements for the plain concrete.

stress value equal to $f_t$. Once the separation starts to increase, there will be a decrease in bonding stress. When it reaches a limit value of separation ($\delta_p$), the bonding stress tends to zero. In the actual implementation of this model, the separation of adjacent element edges is assumed in advance by introducing joint elements and describing the topology of adjacent elements with different nodes. As no two elements share any nodes the continuity between elements is enforced through the penalty function method. Before the bonding stress reaches the tensile strength its value is given by equation (1), where $\delta_t$ is the separation corresponding to when the bonding stress is equal to the tensile strength ($\delta_t = 2h\ f_t/p$), $h$ is the size of that particular finite element and $p$ is the penalty parameter.

$$\sigma = f_t\ \left[\frac{2\delta}{\delta_t} - \left(\frac{\delta}{\delta_t}\right)^2\right] \tag{1}$$

After the bonding stress has reached the tensile strength, the strain-softening law described in terms of stress and displacements is given by the equation (2), with a heuristic scaling function representing an approximation of the experimental stress-displacement curves and the parameters $a = 0.63$, $b = 1.8$ and $c = 6$ are obtained from the interpolation of experimental stress displacement curves. These parameters only define the shape of the softening curve, which is then stretched depending on the material properties of the material (i.e. the energy release rate and the tensile strength). However, the heuristic curve that was implemented in the first Y-code was derived from direct tension experiments on concrete samples. There are other materials that have been tested to obtain a more representative softening curve shape, such as granite, e.g. see [28]. The variable D is given by equation (3) and the complete relationship for the normal bonding stress as a function of separation can be written as shown in equation (4).

$$\sigma = f_t \ \frac{1 - \frac{a+b-1}{a+b} e^{\left( D \frac{a+cb}{(a+b)(1-a-b)} \right)}}{\left[ a\left(1-D\right) + b\left(1-D\right)^c \right]^{-1}} \tag{2}$$

$$D = \begin{cases} 0 & \delta \leq \delta_t \\ \frac{\delta - \delta_t}{\delta_p - \delta_t} & \delta_t \leq \delta \leq \delta_p \\ 1 & \delta > \delta_p \end{cases} \tag{3}$$

$$\sigma = \begin{cases} f_t \ \frac{2\delta}{\delta_p} & \delta < 0 \\ f_t \ \left[ \frac{2\delta}{\delta_p} - \left( \frac{\delta}{\delta_p} \right)^2 \right] & 0 \leq \delta \leq \delta_t \\ f_t \ \frac{1 - \frac{a+b-1}{a+b} e^{\left( D \frac{a+cb}{(a+b)(1-a-b)} \right)}}{\left[ a(1-D) + b(1-D)^c \right]^{-1}} & \delta > \delta_t \end{cases} \tag{4}$$

## 4.2 Fibre reinforced sprayed concrete

The fracture mechanism involved in the fibre reinforced spayed concrete is affected by the presence of discrete fibres in the concrete matrix. Although the presence of fibres increases the fracture process zone size, neither the tensile strength nor the early post-peak behaviour are assumed to be influenced by the presence of fibres at low volume fractions. Figure 7 shows the modified stress-opening relation that has been implemented in the code to account for the concrete cracking, fibre de-bonding, and fibre pull-out. The concrete matrix fracture mechanisms dominate the post-peak behaviour for small crack opening. For this reason, the stress, after reaching the value of tensile strength ($f_t^c$), follows the relation for the plain concrete with the previous exponential softening curve defined by equation (2) up to a crack opening of $\delta_p^f$, defined in equation (5). The value of crack opening $\delta_p^f$ is reached when the fibres in the concrete matrix are activated. At the beginning of the fibre pull-out phase, the bonding stress between two fracture walls is defined by the post-crack residual strength $f_t^f$. The stress then decreases linearly with the crack opening $\delta$, up

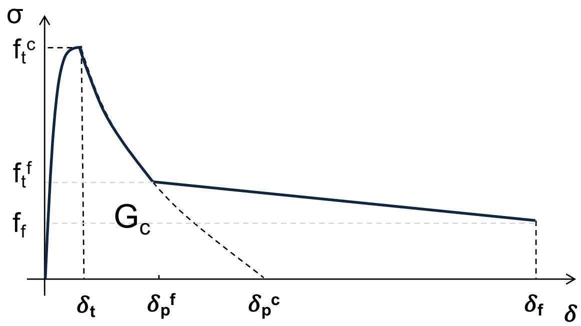


Figure 7. Strain softening defined in terms of displacements for the fibre reinforced sprayed concrete.

to a value of $f_f$, corresponding to the crack opening limit $\delta_f$. The complete relationship for the normal bonding stress as a function of separation is shown in equation (6).

$$\delta_p^f = 3\ G_c \frac{1 - \frac{f_t^f}{f_t^c}}{f_t^c + f_t^f} \tag{5}$$

$$\sigma = \begin{cases} f_t^c\ \frac{2\delta}{\delta_p^c} & \delta < 0 \\ f_t^c\ \left[\frac{2\delta}{\delta_p^c} - \left(\frac{\delta}{\delta_p^c}\right)^2\right] & 0 \leq \delta \leq \delta_t \\ f_t^c\ \frac{1-\frac{a+b-1}{a+b} e^{\left(\frac{(\delta-\delta_t)(a+cb)}{(\delta_p^c-\delta_t)(a+b)(1-a-b)}\right)}}{\left[a\left(1-\frac{\delta-\delta_t}{\delta_p^c-\delta_t}\right)+b\left(1-\frac{\delta-\delta_t}{\delta_p^c-\delta_t}\right)^c\right]^{-1}} & \delta_t \leq \delta \leq \delta_p^f \\ \frac{f_t^f-f_f}{\delta_p^f-\delta_f}\ (\delta - \delta_p^f) + f_t^f & \delta_p^f \leq \delta \leq \delta_f \\ 0 & \delta > \delta_f \end{cases} \tag{6}$$

The constitutive laws for the joint-elements that have been defined in this section can be represented as the interposition of normal and shear springs between the joint nodes of the elements in contact, as shown in Figure 8. The normal springs have a non-linear stress displacement law given by equation (4), whereas the shear springs have analogous laws representing shear failures. The normal and shear springs between the joint nodes of the elements in contact are removed once the separation reaches the value $\delta_f$, meaning that the fracture has propagated through the edge.

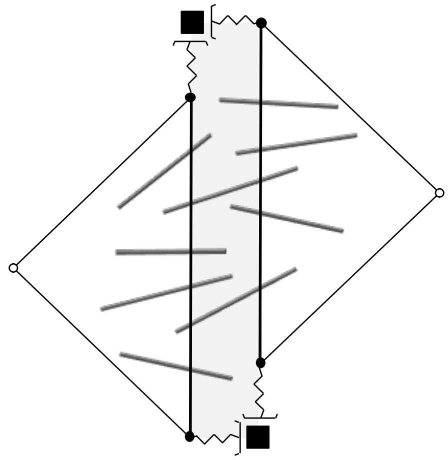

Figure 8. Schematic representation of the joint-elements: normal and shear springs transmit the residual bonding stress between the edges of two finite elements during concrete cracking, fibre de-bonding, and fibre pull-out.

# 5 Three-point bending test simulations

## 5.1 Numerical model

The implemented joint-element constitutive model has been validated by comparing the simulated response with the experimental data for three bending tests on plain and FRC beams reported in [3]. The geometry of the tested samples is shown in Figure 9(a).

The experiments have been modelled with 2D FEMDEM simulations. The boundary conditions and the 2D triangular mesh are illustrated in Figure 9(b). The top roller is constrained with constant velocity. To reduce the run time of the numerical simulation, the velocity of the constraint is set to 0.01 m/s. Although this loading rate is higher than the one in the laboratory experiment, it induces a quasi-static response in the bar as there is no significant difference between the force applied by the punch and the one applied by the two constraints. To further reduce the calculation time, when the simulation starts, the roller is in contact with the specimen. Since fracture initiates and propagates above the notch, the specimen is discretised with an unstructured coarse mesh at the two edges. Moreover, a fine mesh is employed in the centre of the specimen to better represent both the de-bonding stress during the opening of the crack and the fracture path along the element boundaries. The total number of elements employed in the model is around 2,200. The material properties used to describe the three-point bending apparatus are $\mathrm{E_s}$=210 GPa, $\nu_\mathrm{s}$=0.3 and $\rho_\mathrm{s}$=7850 kg/m$^2$, where $\mathrm{E_s}$ is the Young's modulus, $\nu_\mathrm{s}$ is the Poisson's ratio and $\rho_\mathrm{s}$ is the density. The material properties used for the specimens are $\mathrm{E_c}$=26.5 GPa, $\nu_\mathrm{c}$=0.19, $\rho_\mathrm{c}$=2333 kg/m$^3$, $\mathrm{f_t}$=3 MPa and $\mathrm{G_I}$=90 J/m$^2$. The frictional interaction between the rollers and the samples is modelled using a Coulomb coefficient of friction equal to 0.01. The parameters that describe the FRC post peak behaviour due to its fibres are $f_f^t = f_f = 0.5$ MPa and $\delta_f = 3.5$ mm.

## 5.2 Results

Results from the FEMDEM simulations on plain and fibre-reinforced concrete and the corresponding experimental load-CMOD curves of three bending tests on the two types of concrete are shown in Figure 11. The numerical results for the plain concrete specimens are compared with the corresponding experimental curves in Figure 11(a). The value of the peak load is correctly represented in the simulated experiment. The numerical model slightly overestimates the load in the initial part of the post peak load-CMOD curve and underestimates the load after a CMOD of about 0.2 mm. This is difference is due to the values of the parameters $a$, $b$ and $c$ that have been chosen to represent the decay of the concrete stiffness during crack propagation.

Overall, the behaviour of the actual plain concrete specimens is well represented in the corresponding numerical simulation, with an ultimate CMOD of 0.8-0.9 mm. Figure 11(b) shows the results for the FRC specimens. Here the numerical results match very well the experimental data, not only in terms of peak load, but also for the residual strength during fibre de-bonding and fibre pull-out.

Figure 10 shows the difference in the horizontal stress filed for the two types of concrete for an equivalent fracture width. In the plain concrete beam, the two fracture walls are unloaded, as shown in Figure 10(a). Differently, in the FRC beam shown in Figure 10(b), even though the fracture has almost split the specimen in two halves, the fracture walls are still joined by some steel fibres and the cracked section is under horizontal stress, in order to support the applied load that is transmitted by the punch.

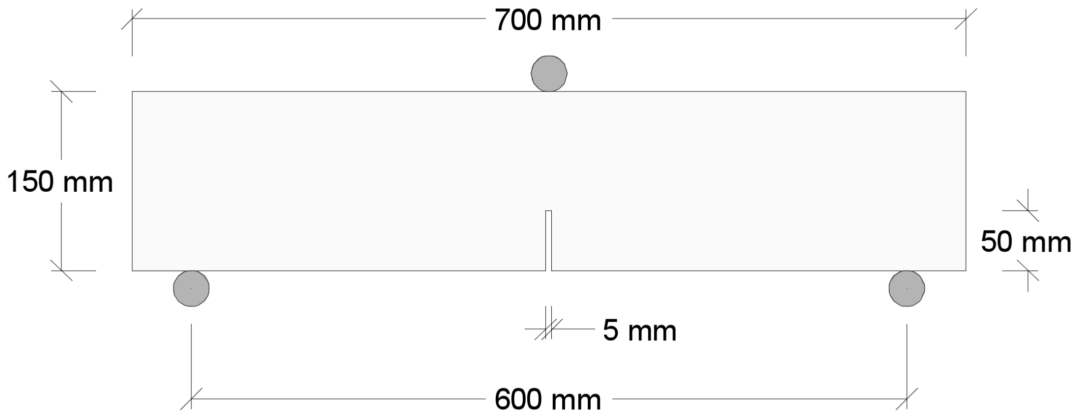


(a)

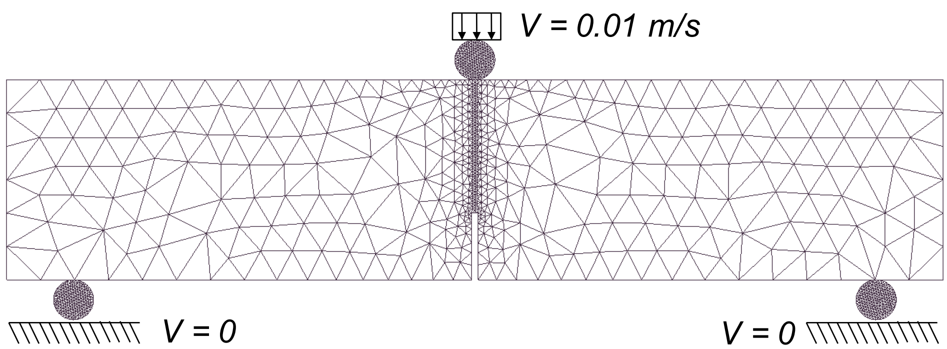


(b)

Figure 9. a) Geometry of three-point bending specimens that have been tested in [3]. b) Mesh and boundary conditions of the same beam that have simulated using FEMDEM.

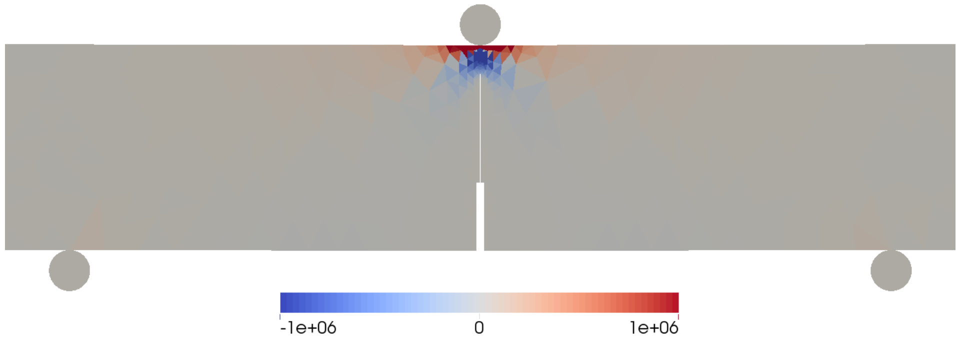


(a)

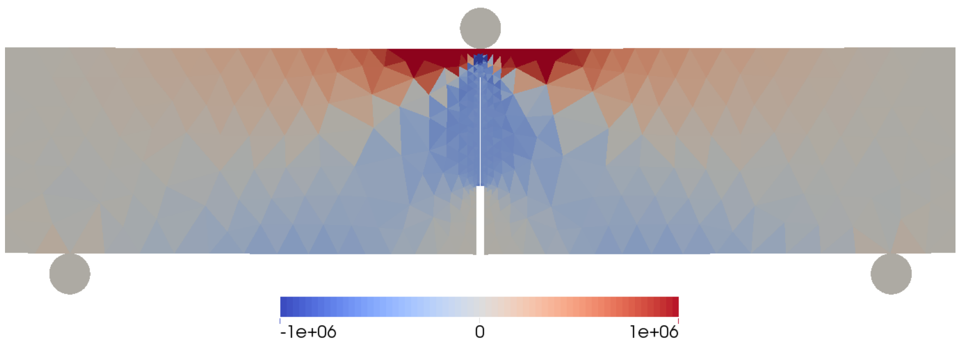


(b)

Figure 10. Horizontal stress [Pa] in the simulated a) plain and b) FRC beams with the joint-element constitutive model implemented in FEMDEM.

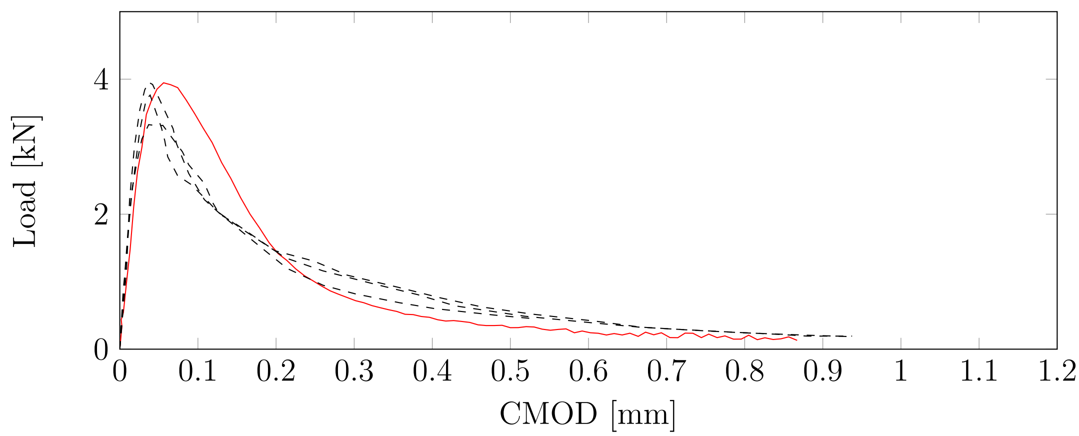


(a)

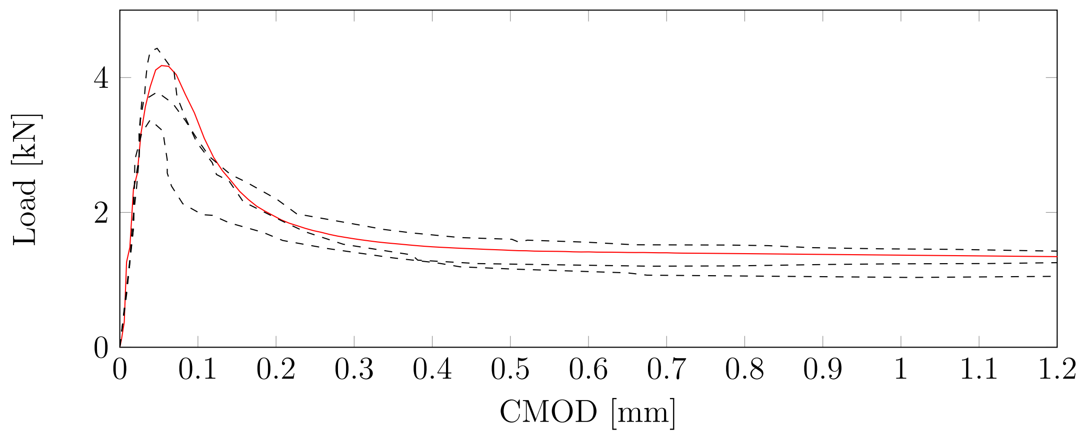


(b)

Figure 11. Experimental results (dashed black) for three bending tests on a) plain and b) FRC beams [3]. Numerical response (red) of the simulated a) plain and b) FRC beams with the joint-element constitutive model implemented in FEMDEM.

# 6 Tunnel simulations

## 6.1 Numerical model

The new joint-element constitutive model has been applied to simulate the response of two FRC tunnels. The geometry and mesh of the simulated circular tunnel is shown in Figure 12(a), whereas the typical NATM tunnel shape, which is that of the Heathrow Trial Tunnel (HTT) [40] is illustrated in Figure 12(b). The tunnels have been modelled with 2D FEMDEM simulations. The two tunnels are subjected to increasing in situ stresses: the vertical stress is ramped from 100 kPa to a value of 1 MPa. The horizontal stress is ramped from 40 kPa to 400 kPa. Although the FEMDEM code is capable of simulating the interactions between the soil and the tunnel linings, the effects of the in situ soil stresses and subsequent passive reaction have been directly applied to the linings as an equivalent surface pressure. This has been done to reduce the run time of the simulations.

A fine mesh is employed for the linings to better represent the de-bonding stress during the opening of the crack. The refinement of the triangular mesh employed for the tunnels is illustrated in Figure 12(c). The total number of elements employed in the model is around 36,100. The material properties used to describe the soil (London Clay) are $E_s$=125 MPa, $\nu_s$=0.2 and $\rho_s$=2000 kg/m$^2$, where $E_s$ is the Young's modulus, $\nu_s$ is the Poisson's ratio and $\rho_s$ is the density. The material properties used for the linings have been reported in the previous section.

## 6.2 Results of circular tunnel shape

Figure 13 shows the horizontal stress field and fracture surfaces for the numerical simulations of the plain concrete and FRC circular tunnel under ramping in situ stresses. Fractures appear with an in situ vertical stress between 450 and 600 kPa in the inner arch at the top and bottom of the linings. Figure 13(c) and 13(e) show the fractured sections of the plain concrete lining. After failure, the stress around the cracks drops to zero, meaning that that portion of the tunnel is not supporting the in situ stresses. Differently, the fibres in the fractured sections of the FRC lining are still transmitting some stress in order to equilibrate the in situ stresses, as shown in Figure 13(d) and 13(f). The horizontal stress at the bottom and top inner arch of the tunnel is

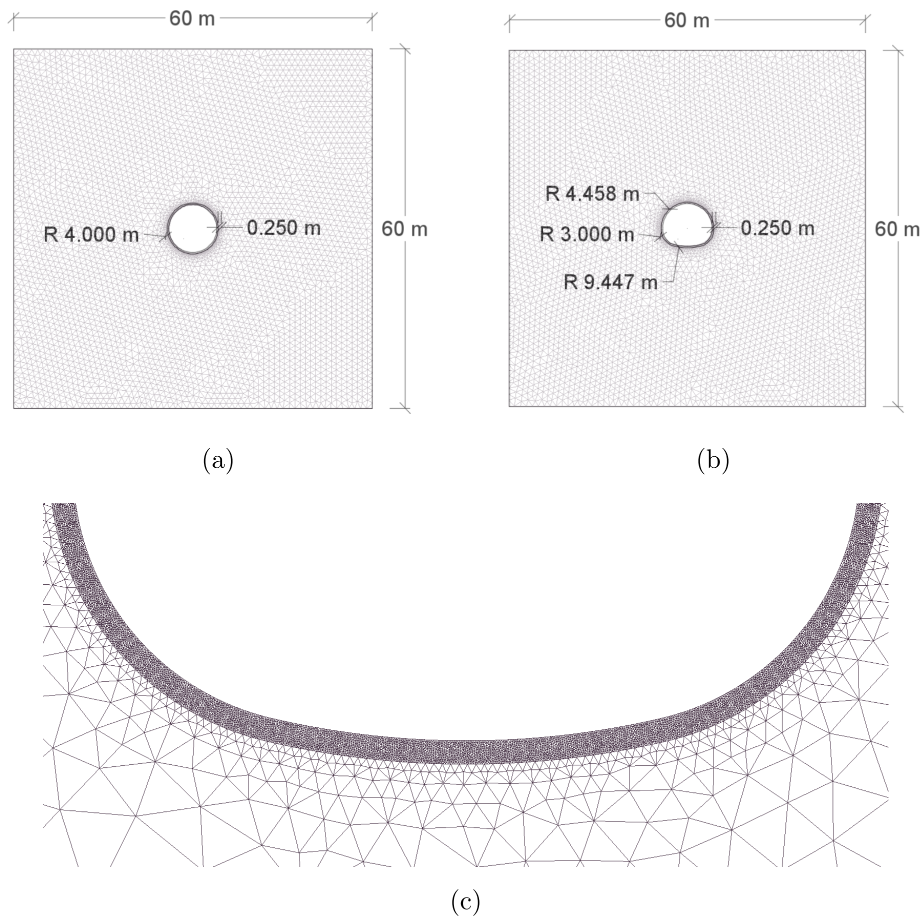


Figure 12. Geometries and finite element mesh of a) the circular and b) complex-shaped tunnel that have been analysed using FEMDEM. c) Detail of the mesh discretisation used for the complex-shaped tunnel.

plotted against the applied in situ vertical stress in Figure 14. The numerical results show that cracking is more localised for the plain concrete lining (with a crack spacing of about 180-200 mm) compared to the FRC (with a crack spacing of about 120-160 mm). The stress in these most vulnerable sections of the lining increase with the applied in situ stresses, up to the value of tensile strength (3 MPa). At that point the stress carried by the plain concrete drops to zero, whereas reaches the value of the residual strength (0.5 MPa) in the FRC.

Figure 15 shows the results of a similar analysis undertaken with finite elements (FE). This figure shows the areas where the model predicts tensile stresses in the tunnel lining. The finite element model implements the non-linear stress strain curve of FRSC previously shown in Figure 4(a).

Comparing the FE analysis results with the FEMDEM analysis, it is apparent that the areas and magnitudes of stress predicted by both are comparable. However, the FE model is not able to capture the crack initiation and propagation. Thus crack widths, spacings and locations are not able to be captured with this 'smeared' approach to modelling cracking.

## 6.3 Results of Heathrow Trial Tunnel shape

Figure 16 shows the horizontal stress field and fracture surfaces for the numerical simulations of the plain concrete and FRC HTT shape under ramping in situ stresses.

Fractures appear with an in situ vertical stress around 400 kPa. The plain concrete lining in Figure 16(a) shows a single crack in the centre of the inner bottom arch of the tunnel. High tensile stresses also occur on the extrados of the lining at the 'knees'. The FRSC lining in Figure 16(b) shows a more distributed crack pattern due to stress redistributions and post crack ductility provided by the fibres. In this case, the fibres have been activated to keep the structure together. There is a certain degree of asymmetry in the results due to the fact that the computational mesh is not symmetric with respect to the vertical axis.

Figure 17 shows the results of a similar analysis undertaken with finite elements (FE), similar to the circular tunnel. As with the circular shape, the FE analysis predicts similar stresses to the FEMDEM analysis, and again the FE model is not able to capture the crack initiation and propagation. Moreover, the zone of tensile stresses on the extrados at the knees of the lining in the FE model is slightly above the locations identified in the FEMDEM

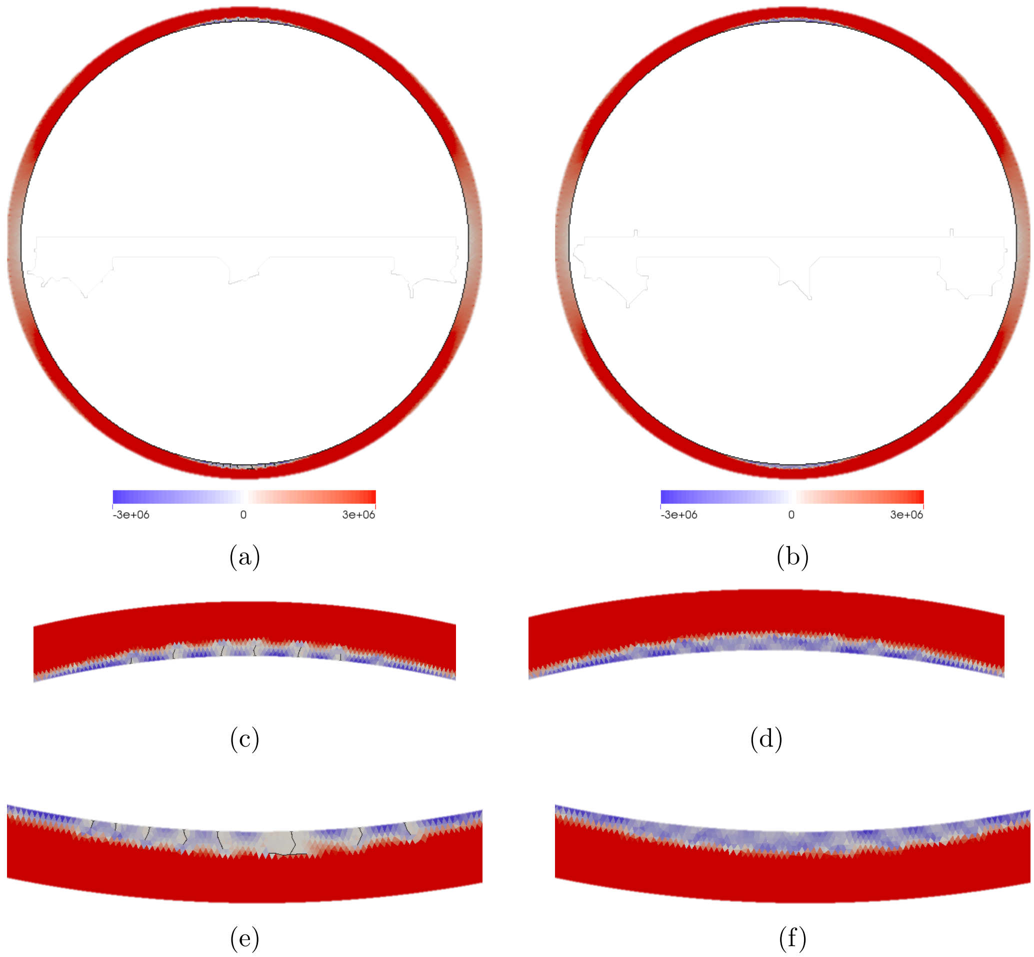


Figure 13. Horizontal stress [Pa] in the simulated a) plain and b) FRC circular tunnel with the joint-element constitutive model implemented in FEMDEM. Details of the damaged zones in c) the upper and e) the bottom inner arch of the plain concrete tunnel, and of the FRC lining d) and f) respectively.

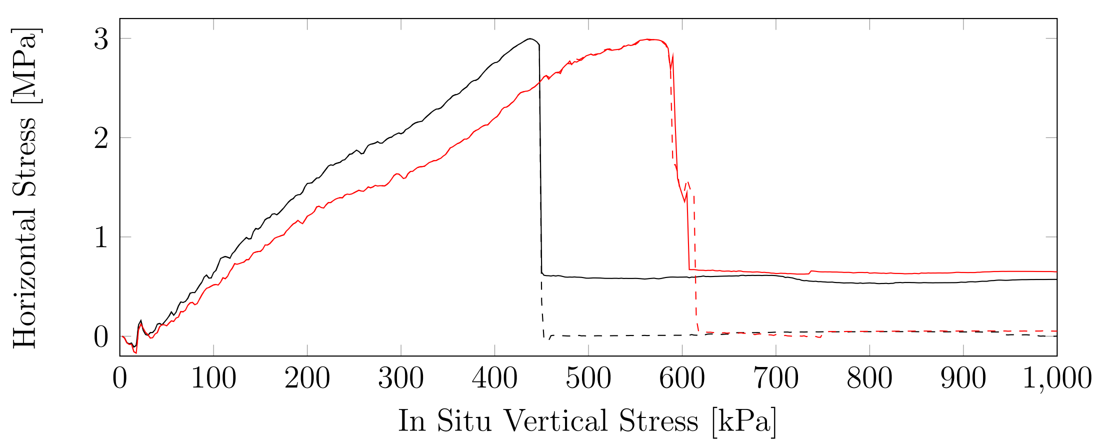


Figure 14. Numerical response of the simulated plain (dashed) and FRC (continuous) tunnels with the joint-element constitutive model implemented in FEMDEM. The horizontal stress at the bottom (black) and top (red) inner arch of the tunnel is plotted against the applied in situ vertical stress.

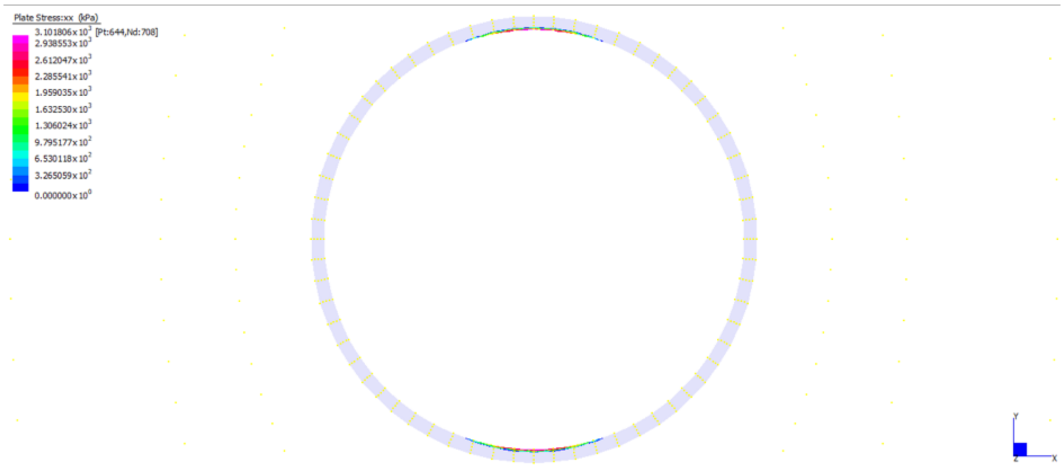


(a)

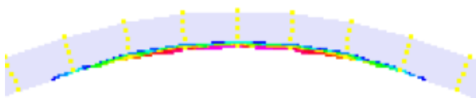

(b)

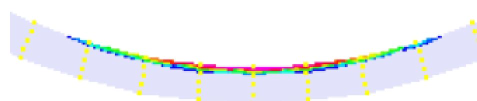

(c)

Figure 15. a) Areas of horizontal tensile stress [kPa] in circular tunnel predicted by finite element analysis. Details of the damaged zones in b) the upper and c) the bottom inner arch.

simulation. This is likely to be due to the stress redistribution around discrete cracks that is modelled with FEMDEM code but 'smeared' by the FE code.

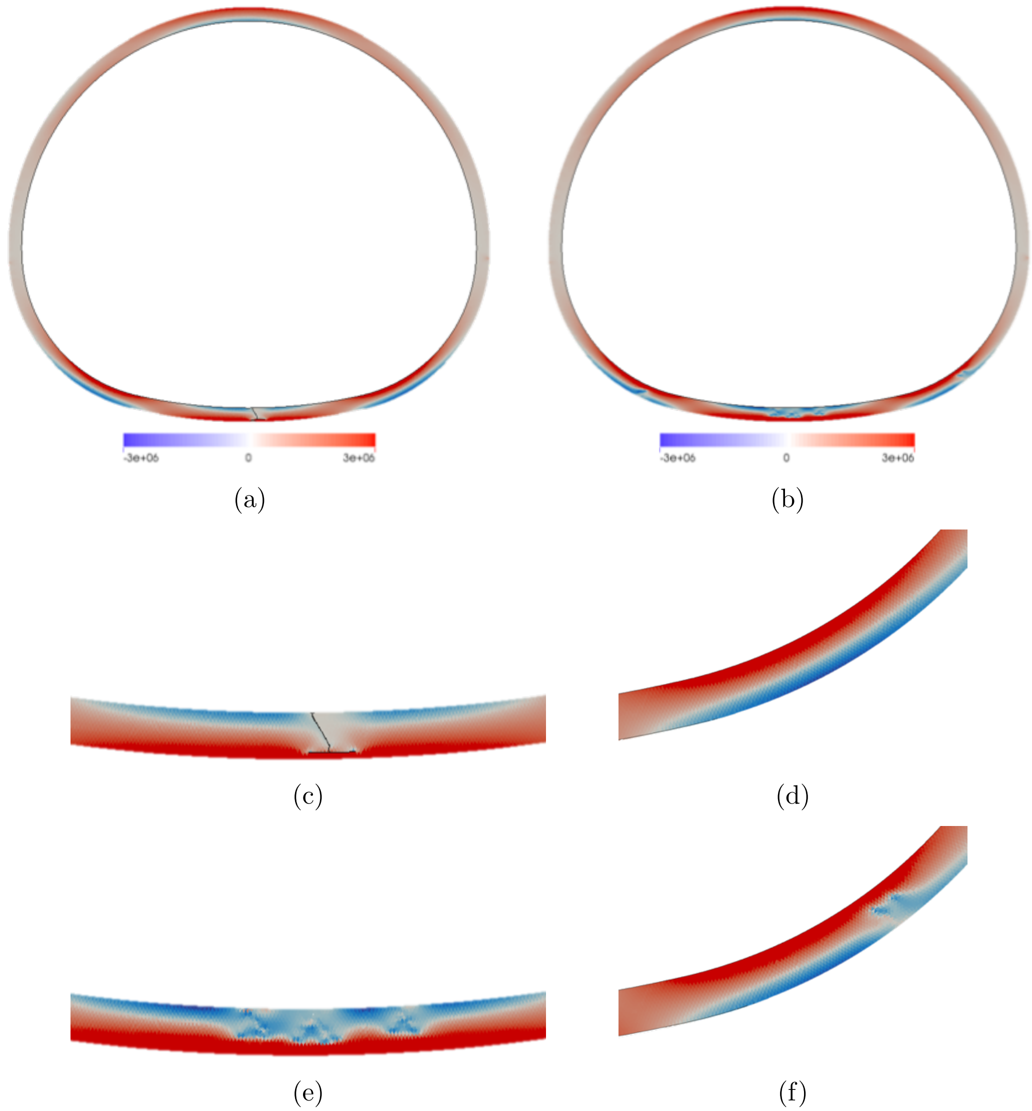


Figure 16. Horizontal stress [Pa] in the simulated a) plain and b) FRC HTT tunnel with the joint-element constitutive model implemented in FEMDEM. Details of the damaged zones in the bottom inner arch: c) plain concrete and d) FRC lining. Details of the bottom right outer arch: d) plain concrete and f) FRC lining.

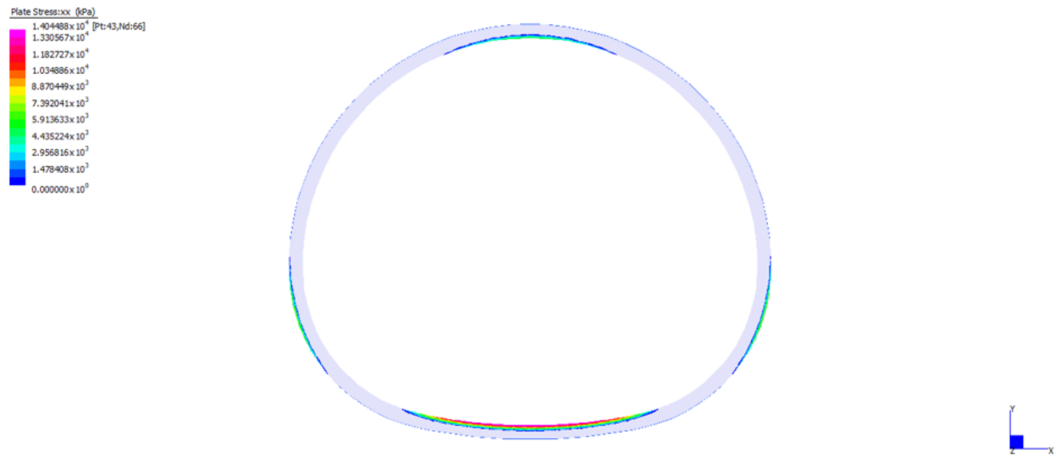


Figure 17. Areas of horizontal tensile stress [kPa] in Heathrow Trial Tunnel shape predicted by finite element analysis.

### 6.3.1 Comparison with prior physical modelling studies

The FEMDEM analysis of the plain concrete model for the Heathrow Trial Tunnel shape showed that as the ground loads were increased, cracking occurred in the invert. If the loading were continued, failure of the tunnel would have occurred as the crack propagated the full depth of the lining.

A previous study undertaken by Staerk (2002) [41] used physical modelling of the Heathrow Trial Tunnel shape to investigate the likely failure mechanism of tunnel linings. This study applied similar boundary conditions to the FEMDEM study, incrementally increasing vertical and horizontal ground stresses until the lining fractured (Figure 18). The lining was made of chalk which behaves as an elastic-brittle material, similar to plain concrete.

The failure mechanisms of both the FEMDEM and physical study are remarkably similar. Both show initiation of a single large crack in the invert which propagates through the lining. This comparison demonstrates the potential for FEMDEM to be applied to capture the failure mechanisms in tunnel linings. Furthermore, given the new joint element constitutive model implemented in this study, there is merit in exploring how the use of fibres in the tunnel lining can improve the ultimate limit state loading that tunnel linings can sustain. Additionally, the ability of FEMDEM to model crack initiation and fracture pattern under increasing load would allow detailed investigation of likely crack widths, spacing and their location. This would ultimately allow tunnel lining designers to produce robust and efficient FRSC linings.

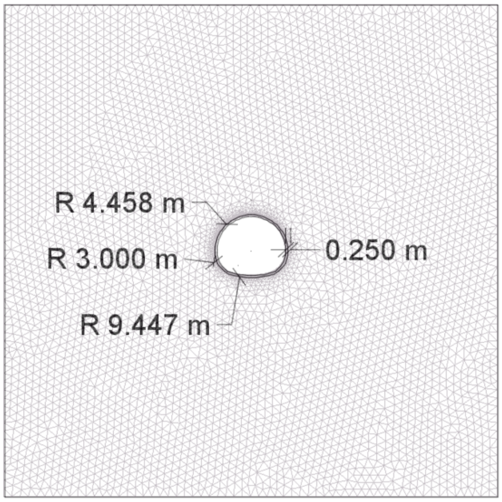


(a)

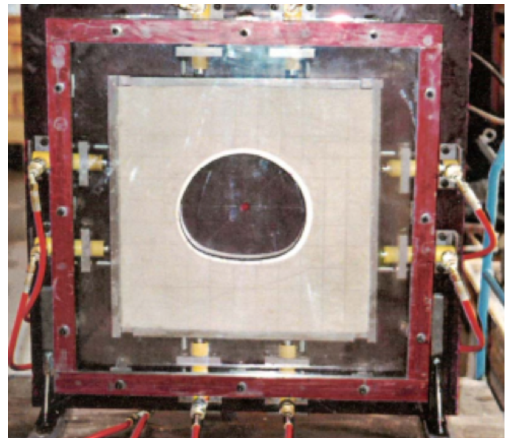

(b)

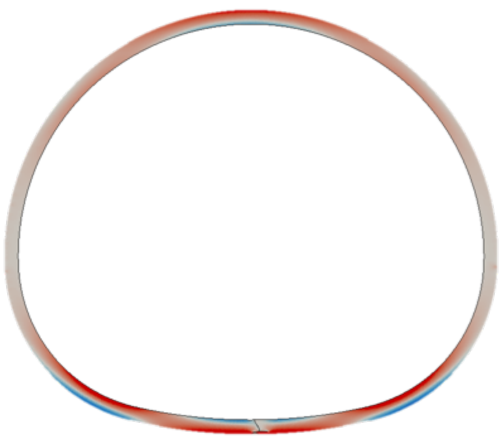

(c)

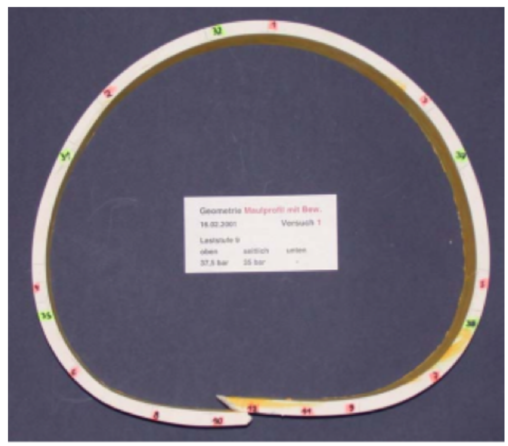

(d)

Figure 18. a,b) Comparison of FEMDEM and physical test boundary conditions. c,d) Comparison of predicted fracture between FEMDEM and physical test.

# 7 Discussion

In the bonding stress model that has been described above, the stress and strain fields close to the crack tip are influenced by the magnitude and distribution of the bonding stress close to the crack tip. In particular the stress field is influenced by the mesh topology close to the crack tip. For this reason, in order to obtain accurate numerical representations of the stress relaxation during fracture propagation, a sufficiently fine mesh needs to be used. Since each joint-element transmits a constant value of bonding stress, at least four elements should be used to discretise the plastic zone during the crack opening. The size of the plastic zone, which is the portion of material that is deforming under stresses that have reached the value of the tensile strength, is defined by the material properties of the simulated structure (Young's modulus, fracture toughness and tensile strength) and is normally of the order of few millimetres for standard concretes. For many engineering applications, when a system of dozens of meters is simulated, this constraint on the mesh size might be impractical as it would extend too much the runtime of the simulations. For this reason a coarser mesh is often employed when simulating big systems, reducing the accuracy of the calculations.

The mesh size is not the only constrain on the numerical discretisation of the simulated body. The fracture path is constrained to follow the element edges, where the joint-elements are located. for this reason, since a crack cannot propagate through finite elements but only through their edges, a structured mesh would artificially constrain the cracks to follow some preferential paths. The fracture paths are generally not known a priori, and they should be only governed by the direction of maximum tensile stress at the crack tip. The fracture grows at a crack tip when the stress field reaches the value of tensile strength in the orthogonal direction to the closest joint-element and the cinematic of the structure activated by the external loads needs to allow an opening displacement in that same direction. Unstructured meshes can minimise the mesh dependency on the final crack paths, but the fact that the joint-elements are not necessarily aligned to the direction of maximum stress at the crack tip can cause an artificial overestimation of the structural strength and toughness at the mesoscale.

The code has an explicit solver, in other words it discretises the continuous time in time steps and then it calculates the state of a system at a later time step on the basis of the state of the system at the current time step. This implies that, even if only the status of the system at an exact time is required (e.g. when the tunnel is loaded up to the Ultimate Limit State), the code needs to calculate the output for every prior time step until it reaches the required one. To give an example: if you want to calculate the state of a modelled system after three seconds from the initial conditions, the total run time is equal to the run time of a single iteration multiplied by the number of time steps before the required one, in this case three seconds divided by the length of the time step used for the time integration in the simulation (which is normally in the order of the nanoseconds). At the beginning of the simulation, the whole model is at rest, with zero stress everywhere. This means that the in situ stresses need to be applied during the simulation slowly enough to avoid dynamic effects in the simulated system. In other words, to assure the stability of the simulation, the code needs to calculate the whole system for many time steps. In some cases this makes the run time of a simulation unfeasible.

In spite of the modelling limitations that have been illustrated in this section, the FEMDEM code is capable of capturing the failure mechanisms of FRC structures with a sufficient level of accuracy, as demonstrated in the previous sections. On the one hand, this alone constitutes a considerable improvement from the potentially over conservative continuum methods, such as FEM. These methods do not explicitly capture fracture initiation and propagation and consequently cannot describe with adequate accuracy the stress redistribution in the structure during failure. On the other hand, the discrete representation of fractured portions in the simulated structures allows a quantitative estimation of the damage under a defined loading condition. Not only is it possible to assess the overall performance of the simulated structures, but it is also possible to extract information such as crack widths and crack spacing. This capability of the FEMDEM code can also be useful during tunnel design in order to identify the most vulnerable sections of the lining. Moreover, parametric studies can be done to take into account of uncertainties during the tunnel construction. Parameters such as the variation in the thickness of the lining and actual density of fibres in the mix, can be changed in the simulation to study the serviceability and ultimate limit state behaviour of FRSC tunnel linings under different scenarios.

# 8 Conclusions

In conclusion, the work that has been presented is the first attempt to use a joint-element constitutive model in FEMDEM for the simulation of fracture in FRC structures. The new FEMDEM joint-element constitutive model that has been developed well predicts peak and post crack behaviour of a published data set [3] for plain concrete and fibre-reinforced concrete three-point bending test. The proposed constitutive model is sufficiently versatile to be adapted to any fibre response based on its three-point bending test results.

The FEMDEM code has been applied to a circular and typical SCL lining profile in London Clay loaded up to the Ultimate Limit State. The numerical results show that cracking is more localised for a plain concrete lining compared to the FRC. Some of the limitations of the code have been presented and discussed. Although the FEMDEM code is capable of simulating the interactions between the soil and the tunnel linings, in the proposed examples, the effects of the in situ stresses have been directly applied to the linings as a surface pressure in order to reduce the run time of the simulations.

The simulations that have been shown in this work were limited to FRSC tunnels but the model can be applied to any FRC structure. Continuum methods, such as FEM, do not explicitly capture fracture initiation and propagation and consequently cannot describe with adequate accuracy the stress redistribution in the structure during failure. For this reason they generally give over conservative results.

The proposed method allows the discrete representation of fractured portions in the simulated structures that enables a quantitative estimation of the damage under defined loading condition. For instance it is possible to extract information such as crack widths and crack spacing. The novel techniques employed in this study will help to increase knowledge of the serviceability and ultimate limit state behaviour of FRSC tunnel linings, and so significantly contribute to the development of detailed design guidance for FRSC structures.

The FEMDEM code can be used during tunnel design in order to identify the most vulnerable sections of the lining and therefore to target improved design efficiency. Moreover, parameters such as the variation in the thickness of the lining and actual density of fibres in the mix, can be changed in the simulation to study the serviceability and ultimate limit state behaviour of FRSC tunnel linings under different scenarios. More research needs to be undertaken to reduce the run time of the simulations and model explicitly the interaction between the soil and the FRSC linings.

# 9 Further work and applications of FEMDEM

## 9.1 Multilinear joint-element constitutive model

In the previous sections, the residual strength of fibres has been implemented in the FEMDEM code with a linear degradation of the joint-element stiffness. This allowed the model to correctly simulate the experimental results presented in [3]. In some cases, the post peak behaviour of FRC cannot be described with a linear curve, e.g. when it shows some forms of hardening. With a similar approach to the one presented in the previous sections, more complex stress-opening relations can be described with a multilinear degradation of the joint-element stiffness. There is merit in extending the current implementation of the strain-softening joint element constitutive model to a multi-linear function, which would allow generalisation of the FEMDEM approach. The parameters would then be calibrated to any measured FRSC response. A proposed approach is described herein.

$$\sigma = \begin{cases} f_t^c \, \frac{2\delta}{\delta_p^c} & \delta < 0 \\ f_t^c \, \left[ \frac{2\delta}{\delta_p^c} - \left( \frac{\delta}{\delta_p^c} \right)^2 \right] & 0 \leq \delta \leq \delta_t \\ f_t^c \, \frac{1 - \frac{a+b-1}{a+b} e^{\left( \frac{(\delta-\delta_t)(a+cb)}{(\delta_p^c-\delta_t)(a+b)(1-a-b)} \right)}}{\left[ a\left(1-\frac{\delta-\delta_t}{\delta_p^c-\delta_t}\right) + b\left(1-\frac{\delta-\delta_t}{\delta_p^c-\delta_t}\right)^c \right]^{-1}} & \delta_t \leq \delta \leq \delta_p^f \\ \frac{f_j-f_{j+1}}{\delta_j-\delta_{j+1}} \, (\delta - \delta_j) + f_j & \delta_j \leq \delta \leq \delta_{j+1} \\ 0 & \delta > \delta_f \end{cases} \tag{7}$$

Equation (7) describes a modified multilinear version of the joint-element constitutive model, as shown in Figure 19(a). The $f_j$ and $\delta_j$ parameters can either be directly calculated from uniaxial tensile tests or inferred from load-CMOD curves of bending tests, like the one shown in Figure 19(b). The residual flexural tensile strength $f_j$ at any CMOD can be approximated from the Euler-Bernoulli beam theory with equation (9), in accordance with EN 14651 [1], where $F_j$ are the recorded values of load, $b$ is the width, $l$ is the span length and $h_{sp}$ is the distance between the tip of the notch and the top of the specimen.

$$f_j = \frac{3F_j l}{2bh_{sp}} \tag{8}$$

The crack opening displacement $\delta_j$ corresponding to any value of CMOD, can be calculated assuming *i*) rigid body rotations of the two prism halves centred about the crack tip and *ii*) that the failure occurs along a single dominant crack. An appropriately conservative estimation has been proposed in [42] and can be calculated with equation (9), where $D$ is the total height of the specimen.

$$\delta_j = CMOD_j \frac{0.35\ h_{sp}}{D - 0.3\ h_{sp}} \tag{9}$$

The $f_j$ and $\delta_j$ parameters might also be optimised with inverse analyses to correct the errors introduced by the oversimplified assumptions made for their calculation. For example the Euler-Bernoulli beam equation (9) assumes a linear profile of the stress within the cross-section of the beam. This is definitely not the case for a FRC beam after the peak load, when the fibres are activated in a portion of its cross-section. For this reason, numerical simulations of the bending experiments on fibre-reinforced concrete can be repeated for different values of $f_j$ and $\delta_j$ until the numerical response matches the experimental one.

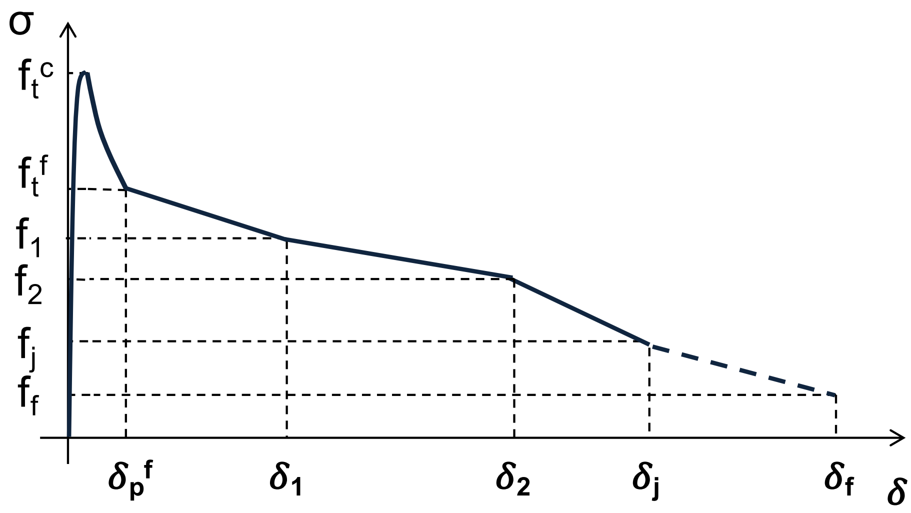


(a)

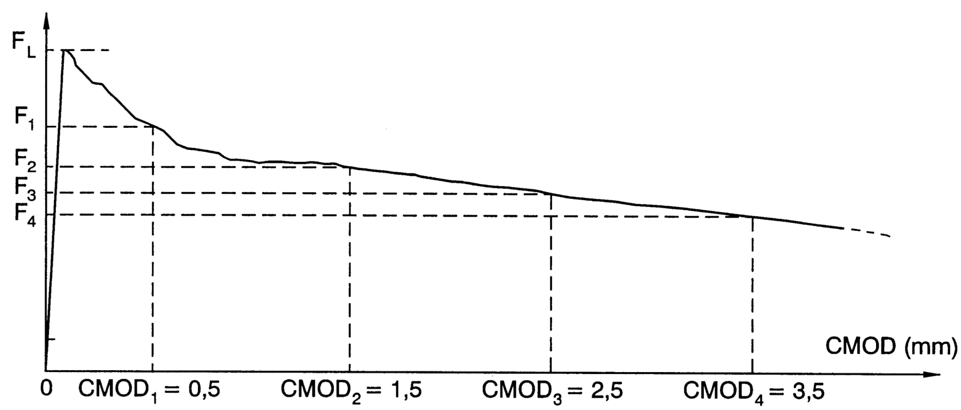


(b)

Figure 19. a) Multilinear residual stress softening relation defined in terms of displacements for the fibre reinforced sprayed concrete. b) Suggested method to calcolate the residual tensile strength of FRC from the load-CMOD diagram [1].

# References

[1] BS EN 14651-2005. Test method for metallic fibred concrete - Measuring the flexural tensile strength (limit of proportionality (LOP), residual), 2005.

[2] A Munjiza. *The Combined Finite-Discrete Element Method*. Wiley, 2004.

[3] Kyoungsoo Park, Glaucio H. Paulino, and Jeffery Roesler. Cohesive fracture model for functionally graded fiber reinforced concrete. *Cement and Concrete Research*, 40(6):956–965, 2010.

[4] HSE. Safety of new Austrian tunnelling method (NATM) tunnels. 1996.

[5] BS EN 14889-1:2006. Fibres for concrete. Steel fibres - Definitions, specifications and conformity, 2006.

[6] Concrete Society Working Group. *TR 63 Guidance for the design of steel-fibre-reinforced concrete*. 2007.

[7] DBV. Merkblatt Stahlfaserbeton, 2001.

[8] Final Recommendation. Test and design methods for steel fibre reinforced concrete: sigma-epsilon-design method - Final recommendation. 36(October):560–567, 2003.

[9] CNR-DT 204. Istruzioni per la Progettazione, l'Esecuzione ed il Controllo di Strutture di Calcestruzzo Fibrorinforzato, 2006.

[10] Comisión Permanente del Hormigón. Ehe-08, 2008.

[11] Comité Euro-International du Béton. fib Model Code, 2010.

[12] EN 1992-1-1:2005. Eurocode 2: Design of concrete structures Part 1-1: General rules and rules for buildings, 2005.

[13] A Paluszny and RW Zimmerman. Numerical simulation of multiple 3D fracture propagation using arbitrary meshes. *Computer Methods in Applied Mechanics and Engineering*, 200(9-12):953–966, feb 2011.

[14] R Borst, JC Remmers, A Needleman, and MA Abellan. Discrete vs smeared crack models for concrete fracture: bridging the gap. *International Journal for Numerical and Analytical Methods in Geomechanics*, 28(78):583–607, jun 2004.

[15] M Jirasek. Nonlocal models for damage and fracture: comparison of approaches. *International Journal of Solids and Structures*, 7683(97):4133–4145, 1998.

[16] BJ Carter. Automated 3-D crack growth simulation. *International Journal for Numerical Methods in Engineering*, 47(1-3):229–253, 2000.

[17] S.A. Silling. Reformulation of elasticity theory for discontinuities and long-range forces. *Journal of the Mechanics and Physics of Solids*, 48(1):175–209, 2000.

[18] S. A. Silling, M. Zimmermann, and R. Abeyaratne. Deformation of a peridynamic bar. *Journal of Elasticity*, 73(1-3):173–190, 2003.

[19] XB Lin and RA Smith. Finite element modelling of fatigue crack growth of surface cracked plates: Part I: The numerical technique. *Engineering Fracture Mechanics*, 63:503–522, 1999.

[20] M Schöllmann, M Fulland, and HA Richard. Development of a new software for adaptive crack growth simulations in 3D structures. *Engineering Fracture Mechanics*, 70:249–268, 2003.

[21] S Bordas and PV Nguyen. An extended finite element library. *International Journal for Numerical Methods in Engineering*, 71(January):703–732, 2007.

[22] TG Sitharam. Numerical simulation of particulate materials using discrete element modelling. *Current Science*, 78(7), 2000.

[23] FA Tavarez. *Discrete element method for modelling solid and particulate materials.* PhD thesis, UNIVERSITY OF WISCONSIN-MADISON, 2007.

[24] HL Huang, EL Detournay, and BL Bellier. Discrete element modelling of rock cutting. In *Vail Rocks 1999*, volume 7, pages 224–230, 1999.

[25] Y Wan. *Discrete Element Method in Granular Material Simulations.* PhD thesis, Technical University of Kaiserslautern, 2011.

[26] D.O. Potyondy and P.a. Cundall. A bonded-particle model for rock. *International Journal of Rock Mechanics and Mining Sciences*, 41(8):1329–1364, dec 2004.

[27] A Munjiza, E Rougier, and EE Knight. Large strain finite element method, 2015.

[28] E Rougier, EE Knight, ST Broome, AJ Sussman, and A Munjiza. Validation of a three-dimensional Finite-Discrete Element Method using experimental results of the Split Hopkinson Pressure Bar test. *International Journal of Rock Mechanics and Mining Sciences*, 70:101–108, sep 2014.

[29] O. K. Mahabadi, G. Grasselli, and A. Munjiza. Y-GUI: A graphical user interface and pre-processor for the combined finite-discrete element code, Y2D, incorporating material heterogeneity. *Computers and Geosciences*, 36(2):241–252, 2010.

[30] O. K. Mahabadi, A. Lisjak, A. Munjiza, and G. Grasselli. Y-Geo: New Combined Finite-Discrete Element Numerical Code for Geomechanical Applications. *International Journal of Geomechanics*, 12(6):676–688, dec 2012.

[31] J Xiang, A Munjiza, and JP Latham. Finite strain, finite rotation quadratic tetrahedral element for the combined finite-discrete element method. *International Journal for Numerical Methods in Engineering*, 79(8):946–978, aug 2009.

[32] A. Munjiza, J. Xiang, X. Garcia, J. P. Latham, G. G Schiava D'Albano, and N. W M John. The Virtual Geoscience Workbench, VGW: Open Source tools for discontinuous systems. *Particuology*, 8(2):100–105, 2010.

[33] N Karantzoulis, J Xiang, B Izzuddin, and J P Latham. Numerical implementation of plasticity material models in the combined finite-discrete element method and verification tests. pages 319–323, 2013.

[34] L Guo. *Development of a three-dimensional fracture model for the combined finite-discrete element method*. PhD thesis, Imperial College London, 2014.

[35] C Joulin, J Xiang, JP Latham, and C Pain. *A New Finite Discrete Element Approach for Heat Transfer in Complex Shaped Multi Bodied Contact Problems*, pages 311–327. Springer Singapore, Singapore, 2017.

[36] J Xiang, JP Latham, and A Farsi. *Algorithms and Capabilities of Solidity to Simulate Interactions and Packing of Complex Shapes*, pages 139–149. Springer Singapore, Singapore, 2017.

[37] J.a.O. Barros and J.a. Figueiras. Model for the analysis of steel fibre reinforced concrete slabs on grade. *Computers & Structures*, 79(1):97–106, jan 2001.

[38] J.A.O. Barros. Post-cracking behaviour of steel fibre reinforced concrete. *Materials and Structures*, 38(275):47–56, 2004.

[39] Lei Mao, Stephanie Barnett, David Begg, Graham Schleyer, and Gavin Wight. Numerical simulation of ultra high performance fibre reinforced concrete panel subjected to blast loading. *International Journal of Impact Engineering*, 64:91–100, 2014.

[40] K H Bowers, D M Hiller, and B M New. Ground movement over three years at the Heathrow Express Trial Tunnel. *Geotechnical Aspects of Underground Construction in Soft Ground*, (1992):647–652, 1996.

[41] Staerk. *Standsicherheitsanalyse von Sohlsicherungen aus Spritzbeton*. PhD thesis, 2002.

[42] Ali Amin, Stephen J. Foster, and Aurelio Muttoni. Derivation of the $\sigma$- w relationship for SFRC from prism bending tests. *Structural Concrete*, 16(1):93–105, mar 2015.